# Contribution of the Crazing Process to the Toughness of Rubber-Modified Polystyrene

**Arminda M. L. Magalhães[†] and Rein J. M. Borggreve*[,‡]**

*Polymer Engineering Center, Universidade do Minho, 4800 Guimarães, Portugal, and DSM Research, P.O. Box 18, 6160 MD Geleen, The Netherlands*

*Received January 31, 1995; Revised Manuscript Received May 17, 1995*[⊗]

ABSTRACT: The deformation process in rubber-modified polystyrene was studied by static SAXS on deformed tensile samples under loaded conditions. The typical scattering pattern of these systems was interpreted as originating from two components: crazing in the polystyrene matrix and a dominant cavitational component associated with the rubbery phase. We have used and checked a new method to separate and quantify the crazing component and to give an estimation of the noncrazing component. The contribution of matrix crazing to the plastic deformation is of minor importance. With an increasing content of rubber, the amount of crazing decreases strongly whereas the (impact) toughness increases. In both PS/SEBS blends and HIPS the main source of plastic energy absorption might be cavitation-induced microscopic shear yielding.

## 1. Introduction

There is general agreement that crazing is a precursor of fracture in glassy homopolymers.[1,2] Crazes nucleate mostly from (surface) imperfections, and polymer fracture is a result of premature craze failure. Although the plastic strain within the fibrils of a craze can be considerable, the very localized nature of a craze implies a low level of energy dissipation and leads usually to a brittle fracture of the material.

On the other hand, many studies report that the toughness of glassy polymers can be increased dramatically by incorporating rubbery particles that promote a large density of crazes.[3,4] Based mainly on dilatometry and transmission electron microscopy studies, the mechanism of absorption of energy was thought to occur principally through multiple crazing of the matrix. The rubbery particles were interpreted as passive stress concentrators able to initiate crazes around the equatorial regions, owing to the large difference in the shear modulus of the matrix and the rubber.[3,5] A certain degree of adhesion between the matrix and the rubbery phase is necessary in order to avoid premature craze breakdown.[6]

So crazes are considered as fracture nuclei in glassy homopolymers and as a source of toughness in rubber-modified glassy polymers. This dualism of the crazing process was put in perspective a few years ago by Bubeck et al., who found that in high-impact polystyrene (HIPS) roughly half of the total plastic deformation is due to crazing.[7–9] Besides crazing of the matrix, voiding or fibrillation of the rubbery phase[10–13] and microscopic shear of the interparticle matrix ligaments[14,15] operate in these materials. These observations were supported by real-time small-angle X-ray scattering (RTSAXS) experiments under tensile impact conditions, which also show that cavitation of rubber particles is preceding matrix crazing and continues until final fracture.[9,15]

Recently, a new model to explain the deformation behavior of rubber-modified crazing matrices was proposed by Bucknall et al.[16,17] The model, which is based on experiments on HIPS, assesses that the rubber particles first cavitate, providing the first nuclei for craze growth, according to the meniscus instability mechanism.[18] Depending on the morphology of the rubber particle, cavitation results in the formation of load-bearing elastomeric fibrils, or a stretched rubber membrane surrounding the cavity. As the crazes extend and thicken, their growth is restrained by the fibrillated rubber (strain-hardening), which takes an increasing share of the applied stress as the strain increases. In this view the main source of energy absorption is still multiple crazing. On the other hand, the results of Gilbert and Donald,[14] Bubeck and co-workers,[9] and Buckley[15] are suggesting that local ligament shearing may have a considerable contribution to the toughness, too.

In order to investigate quantitatively the contribution of both deformation modes to the plastic energy absorption, we studied the deformation process of rubber-modified PS as a function of rubber content and type of rubber. We attempted to separate the crazing and the noncrazing processes (cavitation of the rubber phase, yielding of the glassy ligaments in between rubber particles, etc.) in loaded specimens of rubber-modified PS, using static SAXS on postdeformed samples. Also, a new method of SAXS data analysis is introduced to quantify properly the contribution of crazing.

A commercial HIPS and blends of PS and rubbery triblock copolymers based on polystyrene and hydrogenated polybutadiene (SEBS) were studied. In HIPS the particle morphology depends on polymerization conditions and the internal particle structure is usually not controlled. Incorporation of rubbery styrenic block copolymers as a second phase into a high molecular weight PS matrix has the advantage of combining interfacial adhesion by interpolymer affinity and getting a prescribed morphology of the dispersed phase. The internal morphology of the particle in these systems is determined by the structure of the block copolymer, which in turn depends on the molecular weight and composition of the block copolymer.[19]

## 2. Experimental Section

**2.1. Materials.** Polystyrene (PS N7000) ($M_w$ = 340 000, $M_w/M_n$ = 2.6, $T_{g,DSC}$ = 101 °C), supplied by Shell, was used as the model matrix and was blended with two elastomeric block copolymers. The block copolymers were also purchased from Shell under the trade names Kraton G1651 and Kraton G1652.

[†] Universidade do Minho.
[‡] DSM Research.
[⊗] Abstract published in *Advance ACS Abstracts,* July 1, 1995.

0024-9297/95/2228-5841$09.00/0 

**Table 1. Composition and Microstructure of SEBS Triblock Copolymers**

| designation | $M_w$[a] (kg/mol) total | styrene | rubber | $M_w/M_n$[a] | styrene (%) | $B$[b] (Å) |
|---|---|---|---|---|---|---|
| SEBS-HM: KG 1651 | 177 | 29 | 119 | 1.15 | 32.1 | 610 |
| SEBS-LM: KG 1652 | 49 | 7 | 35 | 1.20 | 28.8 | 270 |

[a] From GPC measurements. [b] $B$ is the center-to-center spacing of the PS glassy domains determined by SAXS.

They are linear triblock copolymers with terminal polystyrene blocks and a middle elastomer block which is hydrogenated from butadiene to a copolymer of ethylene and butylene (SEBS). The two styrenic block copolymers are structurally similar, with comparable nominal composition, but their block lengths and melt viscosities are different. GPC was used to determine the molecular weight of the components. The block copolymers will be referred to as SEBS-HM (KG 1651) and SEBS-LM (KG 1652) based on the differences in overall molecular weight, respectively the high and the low molecular weight block copolymers. The characteristics of the block copolymers used are listed in Table 1.

A high-impact polystyrene, HIPS (Dow Styron XL 8023), containing 7 wt % butadiene rubber in the form of gel particles as generated by bulk polymerization[20] was used. The volume fraction of "composite" rubber particles (with polystyrene inclusions) was estimated to be between 15 and 20%, based on modulus measurements. The average molecular weight of the polystyrene matrix was about 200 000 with a polydispersity of 3.1. A content of 0.5 wt % of mineral oil is present as an additive.

**2.2. Blend Preparation and Morphology.** The blending of PS and SEBS block copolymers was performed in a range of compositions using a Berstorff ZE 25 corotating twin screw extruder with a standard screw geometry at a constant barrel temperature of 240 °C. The extruded strands were quenched and pelletized subsequently. The PS, PS/SEBS blends, and HIPS were injection molded (Arburg Allrounder 220-75-250) at 240 °C into standard tensile and impact test specimens.

The morphology of both HIPS and the PS/SEBS blends was examined with a transmission electron microscope (Philips CM 200) operated at an accelerating voltage of 120 kV. The samples were cryosectioned in a direction parallel to the flow, and the microtomed sections were hardened and stained by exposure to ruthenium tetraoxide ($RuO_4$) vapors using well-described procedures.[21]

Films of pure block copolymers were prepared from the rubber granules by compression molding. The morphology was examined at a direction perpendicular to the film surface, following the same procedure as for the blends.

**2.3. Mechanical Testing and Dilatometry.** Prior to mechanical testing, the specimens were annealed overnight at 80 °C to minimize orientation induced by processing. The mechanical properties of injection-molded tensile specimens (ISO 527-1) were evaluated using a Zwick mode 1445 tensile tester at a strain rate of $1.7 \times 10^{-4}$ s$^{-1}$, unless otherwise stated, at room temperature. The displacement was recorded with an extensiometer. Notched Izod impact strength was determined (ISO 180-1A) using a Zwick impact testing machine in a range of temperature from −60 to +60 °C. The average values of five tests are reported.

To obtain information about the relative adhesion at the interface between PS and a block copolymer, we have used a peel strength method (ASTM D1876) with an ideal peel angle of 90°.[22] In this method, a two-layer sandwich is made by laminating sheets of PS and the block copolymer by compression molding. To prevent stretching of the rubber, a glass fiber cloth is used as backing of the block copolymer. A healing temperature of 170 °C and a healing time of 1 h were selected based on previous studies.[23] The reported value was based on five measurements for each system.

Dilatometry measurements were performed on injection-molded (ISO 527-1) tensile specimens under a constant strain rate of $1.7 \times 10^{-4}$ s$^{-1}$. Two extensiometers were used to measure the longitudinal and the transversal (width) strains, respectively. The thickness strain was assumed to be identical to the width strain. An average value of three specimens was taken for each sample for tests carried out up to 5% longitudinal strain.

**2.4. Microstructure of Deformed Specimens.** The microstructure of deformed samples was studied on thin sections, microtomed from bulk deformed specimens. The sectioning direction was at an angle of approximately 90° to the principal tensile axis to minimize any damage of the craze microstructure.

**2.5. Small-Angle X-ray Scattering.** The SAXS measurements were performed by using a Kratky-type small-angle camera in Cu Kα radiation (wavelength $\lambda = 0.154$ nm) produced by a conventional Philips X-ray generator and collimated with an entrance slit of 30 μm. The diffracted radiation was registered by a position-sensitive detector (M-Braun, Model OED 50). Prior to the scattering measurements, plastic deformation was initiated by drawing the tensile specimens to a certain strain level at a strain rate of $1.7 \times 10^{-4}$ s$^{-1}$. After drawing, the samples were held extended by clamping a specially designed steel jig tightly around the loaded specimen before its removal from the tensile machine. This procedure was necessary because cavitational structures developed during deformation tend to disappear rapidly when the specimen is allowed to relax.[24] For some systems the strain level was taken as a variable. The scattering measurements were obtained with the tensile direction parallel to the length of the Kratky slit. The experimental intensities were corrected for background scattering by subtraction of the scattering curve of the undeformed sample. Each measurement required two runs: a scattering run with the specimen in the scattering position and a transmission run with the specimen in the beam for absorption only. Measured slit-smeared intensities were transformed to an absolute scale by means of a standard polyethylene Lupolen sample (in this paper only slit-smeared intensities are dealt with because desmearing is only possible for isotropic samples).[25,26] The acquisition and analysis of the scattering data were processed using the program FFSAXS.[27]

SAXS experiments have also been carried out with a Kiessig-type small-angle camera. This camera has pinhole collimation and records a two-dimensional X-ray scattering pattern with a photographic film. In this way, the presence of a cross-pattern through the origin, characteristic for crazes,[24-28] was checked.

**2.6. SAXS Data Analysis.** The data analysis was adapted to static SAXS measurements taking into account the reasoning derived in the literature on RTSAXS[9] and involves the following steps:

1. The total plastic strain $\epsilon_T$ was determined from the preimposed strain $\epsilon_A$ (this was done by subtracting the elastic strain $\epsilon_{EL}$, given by the ratio yield stress/tensile modulus, from the preimposed strain). This procedure is allowed since the strain is uniform over the sample gauge length of the tensile bars.

2. The craze volume under the beam and the related plastic strain due to crazing, $\epsilon_{CR}$, were calculated from the analysis of the absolute scattering invariant resulting from the craze fibrils.

3. To obtain the plastic strain due to noncrazing mechanisms (rubber particle cavitation, microscopic shear yielding, etc.), $\epsilon_{CR}$ was subtracted from $\epsilon_T$.

The patterns were analyzed to give information on the small-angle X-ray scattering invariant, $Q$, and the craze microstructure, as measured by the craze fibril diameter, $D$.

**2.6.1. Absolute SAXS Invariant and Volume of Crazes.** The small-angle scattering invariant $Q$ is defined as

$$Q = \int_0^\infty i(q) q \, dq \tag{1}$$

where $i(q)$ is the smeared scattered intensity and $q$ is the magnitude of the scattering vector, defined as $q = (4\pi/\lambda) \sin \theta$, where $2\theta$ is the angle between the incident beam and the direction of scattering and $\lambda$ is the wavelength of the X-rays.

The significance of $Q$ is that its value depends on the volume fraction of the two phases, their electron density difference, and the total volume of scattering centers and not on the structural details, such as the shape and the average dimensions of the two phases.[25] For X-ray radiation incident on crazes, the two-phase system consists of the interconnected void matrix of the craze and the polymer fibrils. The invariant which results from the scattering of crazes is given by[24,29,30]

$$Q = \frac{V}{V_0} v_f (1 - v_f) \Delta\varrho^2 \tag{2}$$

where $V$ is the total volume of crazes illuminated by the X-ray beam, $V_0$ is the total volume of polymer irradiated by the X-ray beam, $v_f$ is the volume fraction of polymer fibrils in the craze, and $\Delta\varrho$ is the difference in electron density between the voids and the polymer fibrils. For a two-phase structure, such as a craze, where the densities of the two phases are known and the volume fraction is estimated from other measurements, the invariant can be used as a measure of total craze volume within the beam.

For small plastic strains, $\epsilon_{CR}$ due to crazing can be related to the craze volume by

$$\epsilon_{CR} = \frac{V}{V_0}(1 - v_f) \tag{3}$$

Combining eqs 2 and 3, the corresponding changes in $\epsilon_{CR}$ can be found from

$$\epsilon_{CR} = \frac{Q}{(\Delta\varrho)^2 v_f} \tag{4}$$

The strain due to deformation events other than crazing (i.e., shear yielding and rubber particle cavitation) is the "noncrazing" strain $\epsilon_{NCR}$, given by

$$\epsilon_{NCR} = \epsilon_T - \epsilon_{CR} \tag{5}$$

**2.6.2. Craze Microstructure.** The mean craze fibril diameter $D$ may be obtained using a Porod analysis[26,30] of the high-angle portion of the scattering curve. The theory of small-angle scattering was first applied to crazes by Paredes and Fischer[31,32] and extensively discussed by Brown and Kramer[24,29] and Dettenmaier.[30] Porod's law states that at the tail end of a small-angle scattering curve, the scattered intensity $i(q)$ should be proportional to $q^{-3}$ for an ideal two-phase system; i.e.

$$i(q) = k_1/q^3 \tag{6}$$

where $k_1$ is the so-called Porod constant, whose value is proportional to the specific surface area of the craze fibrils. The high-angle end of the scattering curve where it is obeyed is called the Porod region. In practice $k_1$ is determined by extrapolating the plot of $i\mathbf{q}^3$ versus $\mathbf{q}^3$ to $\mathbf{q} = 0$ (after subtracting the background far from the beam stop).

The average value of $D$ may be computed from the following expression:

$$D = \frac{Q}{Ck_1(1 - v_f)} \tag{7}$$

where $C$ is a constant and $v_f$ is the fibril volume fraction ($v_f = 1/\lambda_{craze}$) in a craze. A value of the fibril volume fraction $v_f = 0.25$ was assumed based on transmission electron microscopy measurements on polystyrene crazes in thin films.[33]

## 3. Results

**3.1. Morphological and Mechanical Details of the Block Copolymers.** The SEBS copolymers consist of three long segments chemically bonded together. In forming an equilibrium structure, the SEBS copolymers separate into two distinct phases.[34,35] Transmission electron microscopic examination of pure block copolymers SEBS-LM and SEBS-HM reveals a composite structure of a block copolymer consisting of a continuous rubbery phase of hydrogenated polybutadiene and an equilibrium form of predominantly cylindrical microdomains of dispersed glassy polystyrene.

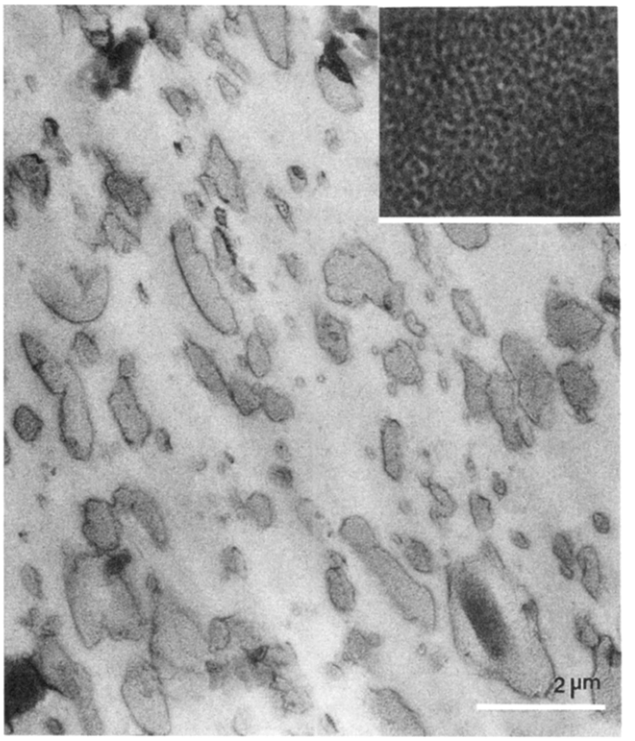


**Figure 1.** Transmission electron micrograph of a thin section prepared by ultramicrotomy of an undeformed bulk specimen of PS/SEBS-HM at 25 wt % block copolymer. As an inset is illustrated the block copolymer internal morphology.

The morphology of the microdomain structure of both block copolymers is similar; only the scale of that structure increases from SEBS-LM to SEBS-HM. Small-angle X-ray scattering (SAXS) experiments support these TEM observations and were used to quantify the microdomain dimensions.

The storage shear modulus, $G'$, was measured with dynamic mechanical analysis (DMA) at a frequency of 0.2153 Hz. SEBS-LM has a modulus of 13 MPa at room temperature, which is significantly higher than the modulus of SEBS-HM (5 MPa). This indicates that the glassy PS domains in SEBS-LM have a higher degree of continuity.

The peel strength between layers of PS and a SEBS block copolymer is respectively 120 N/cm for SEBS-HM and 80 N/cm for SEBS-LM. In both cases the peel strength is considerable, referring to a high amount of energy dissipation during the peeling. The peel test with PS/SEBS-HM shows a cohesive failure in the block copolymer whereas the test with SEBS-LM shows interfacial failure.

**3.2. Blend Morphology.** The typical morphology of the block copolymer modified polystyrene is a result of phase separation between the homopolymer and the block copolymer—*blend morphology*—and a microscopic separation between the incompatible blocks of the copolymer—*internal particle morphology*.

Electron microscopy on some blends indicates that the spherical–cylindrical microdomain geometry inherent to the pure triblock copolymer is retained in the blends. Figures 1 and 2 show the typical morphology of these

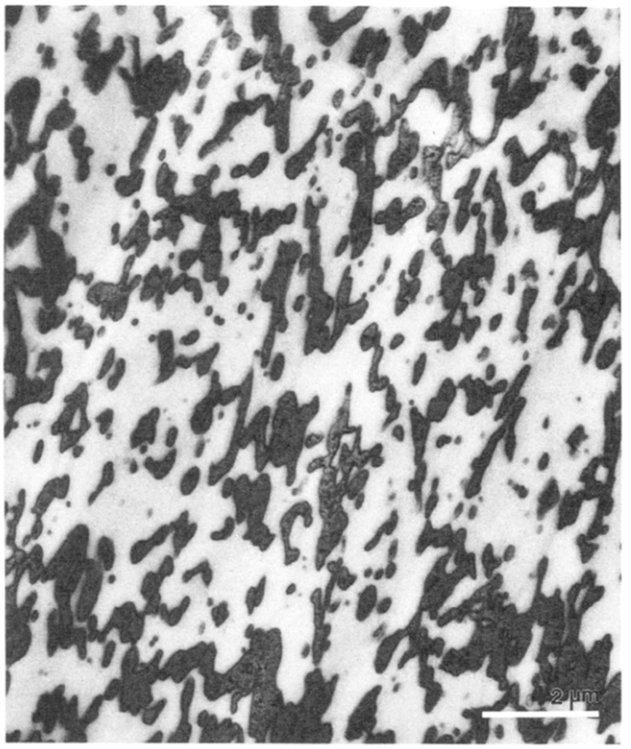


**Figure 2.** Transmission electron micrograph of a thin section prepared by ultramicrotomy of an undeformed bulk specimen of PS/SEBS-LM at 25 wt % block copolymer.

**Table 2. Comparison of Blend Morphology between SEBS-HM and SEBS-LM Blends with Polystyrene**

| block copolymer concn (wt %) | average particle diameter ($\mu$m) | |
|---|---|---|
| | PS/SEBS-HM | PS/SEBS-LM |
| 5 | 1.2 | 0.2 |
| 15 | 1.3 | 0.7 |
| 25 | 1.3 | 1.4 |

blends for a concentration of 25 wt % of the block copolymer.

The examination of the blend morphology shows that the rubber particles are irregular in shape; however, for the compositions investigated an effective average size could be assigned to each system. In the PS/SEBS-HM blends the dispersed particles are spheroidal in shape with a broad distribution of particle size. In the PS/SEBS-LM blends the dispersed phase is more distorted and seems to be somewhat more elongated by the flow field. The particle size (long axis) at the two higher contents of copolymer is roughly the same for both systems, despite the different shapes. These characteristics are summarized in Table 2.

The typical morphology of HIPS is shown in Figure 3. The rubber particles show the multiple inclusion structure (polystyrene occlusions), as a result of the phase inversion in the polymerization step. The average particle diameter is 1 $\mu$m.

**3.3. Mechanical Behavior.** The stress–strain curves for both block copolymer blends, PS/SEBS-LM and PS/SEBS-HM, are depicted respectively in Figures 4 and 5. Summarizing the mechanical behavior, it can be said that both blends undergo yielding at roughly the same stress level, which decreases with the content of block copolymer. The flow stress follows the same trend, resulting in slightly higher values for the blend with SEBS-LM. The elongation of the samples is not accompanied by any significant reduction in cross-sectional dimensions (macroscopic necking) all the way

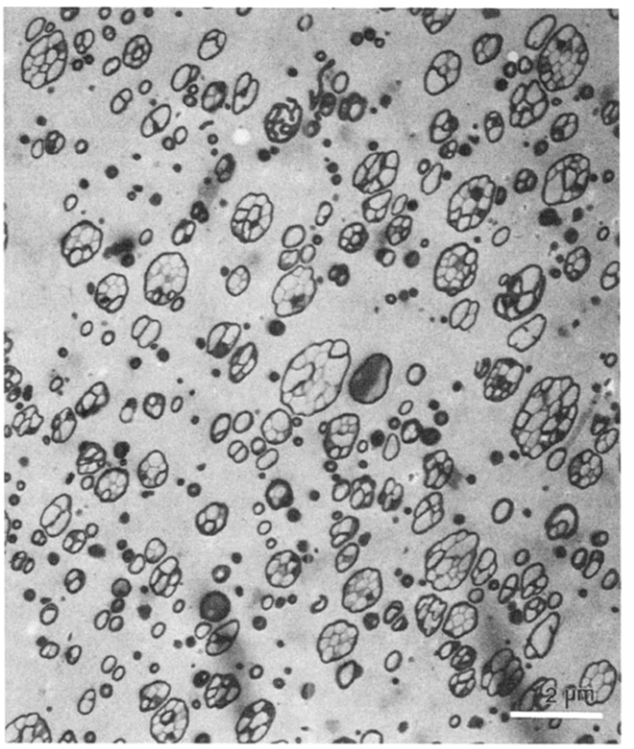


**Figure 3.** TEM of a thin section prepared by ultramicrotomy of an undeformed bulk specimen of HIPS.

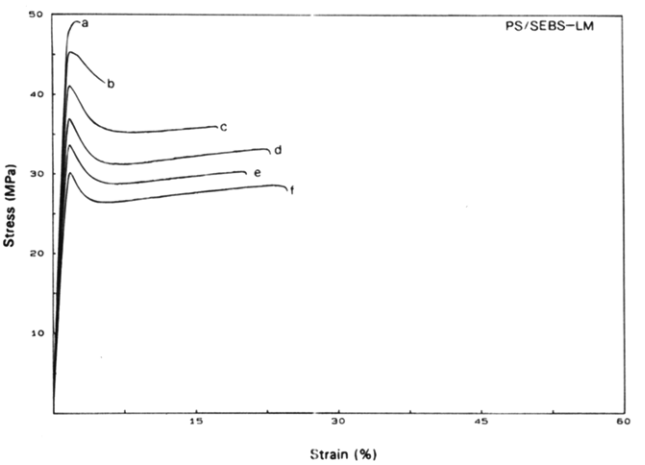


**Figure 4.** Stress–strain curves of PS/SEBS-LM blend at different block copolymer concentrations: (a) 0, (b) 5, (c) 10, (d) 15, (e) 20, and (f) 25%. Tested at room temperature at a strain rate of $10^{-5}$ $s^{-1}$.

up to fracture. Fracture in the blend with SEBS-LM is found to occur at a strain of roughly 30% while that of SEBS-HM is as large as 60% for blends with a copolymer content above 10 wt %. So the strain at break is somewhat smaller for the blends with SEBS-LM.

The dependence of the yield stress and the strain at break on concentration of block copolymer and at different strain rates is shown in Figures 6 and 7, respectively. The expected decrease of the yield stress with rubber content can be observed, a trend which is not influenced by the molecular weight of the block copolymer. However, PS/SEBS-LM has a slightly higher strain rate sensitivity.

It is evident that the ductility improves as the amount of the SEBS added increases, although a tendency to level off is apparent. In the strain rate regime investigated PS/SEBS-HM shows a significant enhancement in ductility at low strain rates. The blend with SEBS-

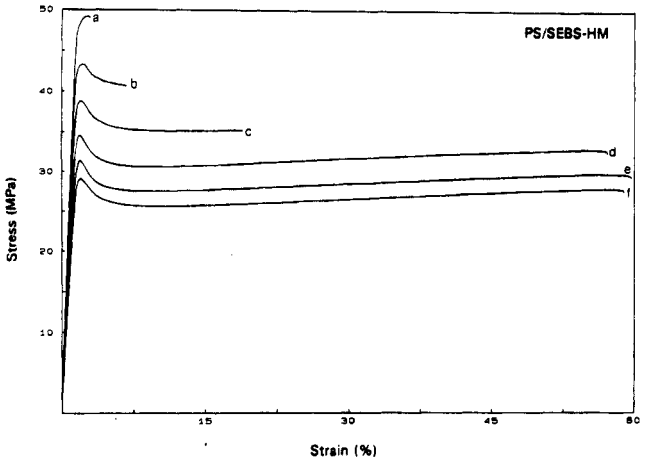


**Figure 5.** Stress–strain curves of PS/SEBS-HM blend at different block copolymer concentrations: (a) 0, (b) 5, (c) 10, (d) 15, (e) 20, and (f) 25%. Tested at room temperature at a strain rate of $10^{-4}$ $s^{-1}$.

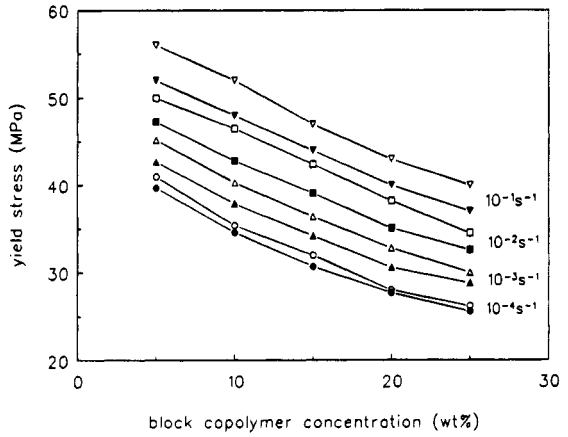


**Figure 6.** Dependence of the yield stress on block copolymer concentration for SEBS-modified PS at different strain rates at room temperature: (a) $10^{-4}$, (b) $10^{-3}$, (c) $10^{-2}$, and (d) $10^{-1}$ $s^{-1}$. The open symbols correspond to SEBS-LM and the solid symbols to SEBS-HM.

LM has a significantly lower strain at break than that of SEBS-HM. A brittle–ductile transition occurs at around 5% block copolymer content.

The results of the notched Izod impact tests are presented in Figure 8. The impact strength of the blends with SEBS-HM is higher than with SEBS-LM over the entire range of temperatures. At low temperatures or low content of block copolymer, the impact strength is reduced to the level of unmodified polystyrene.

The HIPS specimen shows the typical tensile behavior for this material, with characteristic values of 23 MPa for the yield stress and an average strain at break of about 40%, both determined at a strain rate of $1.7 \times 10^{-4}$ $s^{-1}$, and a notched Izod impact strength of 8 kJ/m$^2$ at room temperature.

**3.4. Deformation Behavior. 3.4.1. Dilatometry.** Tensile dilatometry has been used by many investigators to evaluate the deformation mechanisms in rubber-toughened materials.[3,36–39] The individual contributions of cavitational processes (crazing/voiding) and shear yielding can be assessed to some extent by this method. It is assumed that deformations such as voiding and crazing are dilatational processes, which manifest themselves by an increase in volume strain. When shear yielding occurs, a decrease in the volume strain rate is apparent, since plastic deformation occurs

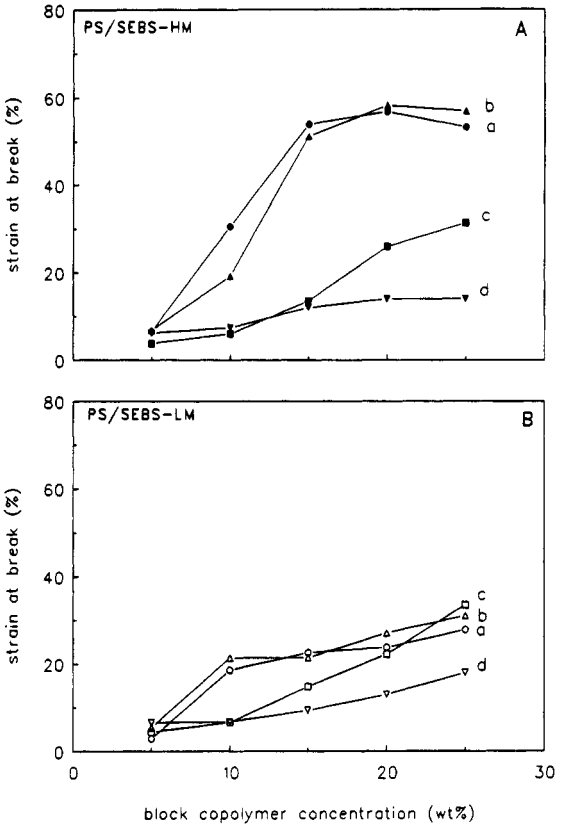


**Figure 7.** Dependence of the strain at break on block copolymer concentration for SEBS-modified PS at different strain rates at room temperature: (a) $10^{-4}$, (b) $10^{-3}$, (c) $10^{-2}$ and (d) $10^{-1}$ $s^{-1}$. The solid symbols correspond to SEBS-HM (A) and the open symbols to SEBS-LM (B).

at approximately constant volume. It has been customary to assume that an increase in volume strain is due entirely to crazing, based on interpretation of post-mortem TEM. However, if both voiding and crazing occur simultaneously, it is impossible to separate their respective contributions to volume strain.

The materials in this study were subject to this test at low strain rate. The results from dilatometry for both PS/SEBS-HM and PS/SEBS-LM are shown respectively in Figures 9 and 10. The initial linear increase in the volume strain below the yield point is due to the elastic behavior. For the two blends, in this region, all the volume strain curves are similar and essentially indistinguishable. When irreversible deformations set in beyond yielding, there is a rapid increase in volume, which increases slightly with increasing addition of block copolymer. The results also suggest that the two types of blends behave quite similarly, although the voiding component is somewhat more pronounced for SEBS-HM, which usually would be interpreted as experiencing more crazing. For both systems, up to the levels of longitudinal strain examined, the measured lateral strains in the specimens are minimum. This suggests that macroscopic shear yielding in PS/block copolymer blends could be neglected (cavitational processes in crazes would make no contribution to the specimen lateral strain). However, it was advanced by some authors that shear in the ligaments between rubber particles does not necessarily imply a change in the lateral dimensions of the sample.[14,15] The global result from these measurements confirms a predominant dilatational component despite the shear and the elastic contributions. Based on traditional interpretations, these results would indicate that the crazing in

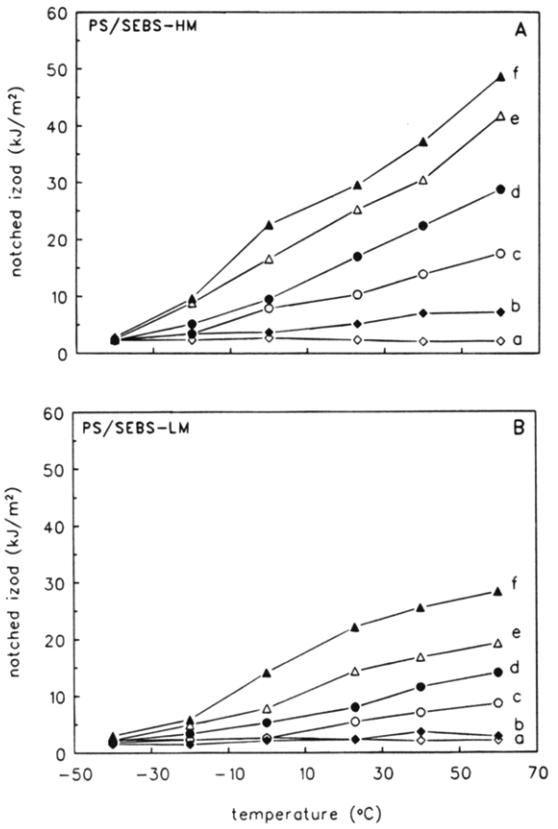


**Figure 8.** Variation in impact strength with temperature and block copolymer concentration for PS/SEBS blends: (a) 0, (b) 5, (c) 10, (d) 15, (e) 20, and (f) 25%. (A) PS/SEBS-HM; (B) PS/SEBS-LM.

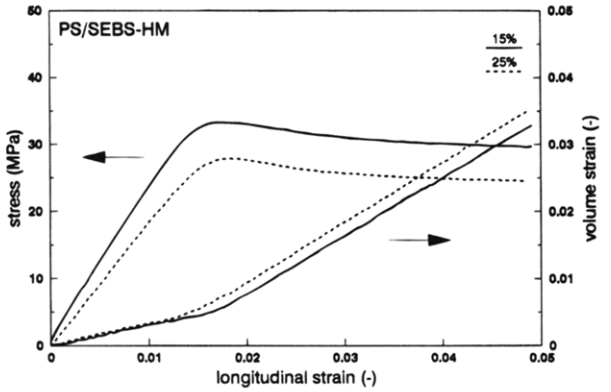


**Figure 9.** Volume strain measurements in tension for SEBS-HM-modified PS at the indicated block copolymer concentration.

the matrix is the predominant mechanism. Nevertheless, observation of cavities in the rubbery phase from TEM micrographs makes this assumption dubious.

**3.4.2. Transmission Electron Microscopy.** The microstructure of the deformed samples was examined by TEM. Figure 11 shows a micrograph of a deformed sample. It demonstrates qualitatively that crazing contributes to the plastic deformation. Also there is evidence that crazes were nucleated or interact with the particles. The cavities in the rubber phase are not readily resolved in the electron micrographs. This might be due to irreversible structural changes following unloading. Examination of the PS/SEBS sections at higher magnifications, however, revealed the existence of cavitation in the rubbery continuous phase of the block copolymer. In the PS/SEBS-LM system with a low

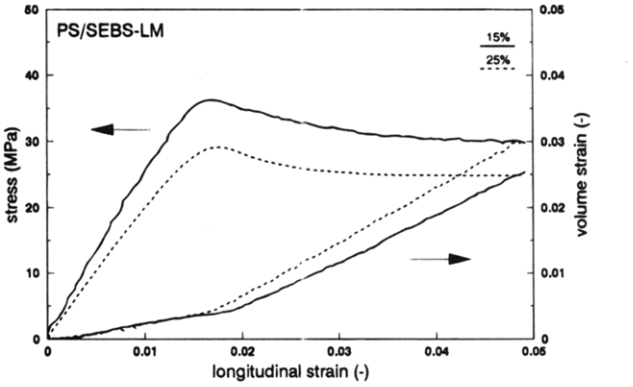


**Figure 10.** Volume strain measurements in tension for SEBS-LM-modified PS at the indicated block copolymer concentration.


**Figure 11.** Transmission electron micrograph of a microtomed section of a deformed PS/SEBS-HM sample. Arrow indicates tensile direction.

content of rubber the available evidence indicates that the few crazes observed seem to initiate entirely from surface stress concentrations (micrograph not shown). This can be due to the inability of small particles in nucleating crazing. In this case the crazes were generally straight, propagating across the entire thickness of the specimen. Qualitatively, with increasing rubber content, crazes nucleating from the composite rubber particles appear to be fewer and shorter.

**3.4.3. Small-Angle X-ray Scattering. 3.4.3.1. Scattering Patterns.** A comparison of a typical scattering pattern of a deformed PS/SEBS blend strained to 5% and the corresponding undeformed system is illustrated for a block copolymer content of 15% and depicted in Figure 12a. As indicated, the pattern of the undeformed specimen shows an interference peak maximum that was related with the block copolymer domains.[40-42] The pattern of the deformed system shows a correlation shoulder that is related with scattering entities developed during uniaxial stretching of the specimen. It can be seen that the X-ray scattering intensity of the

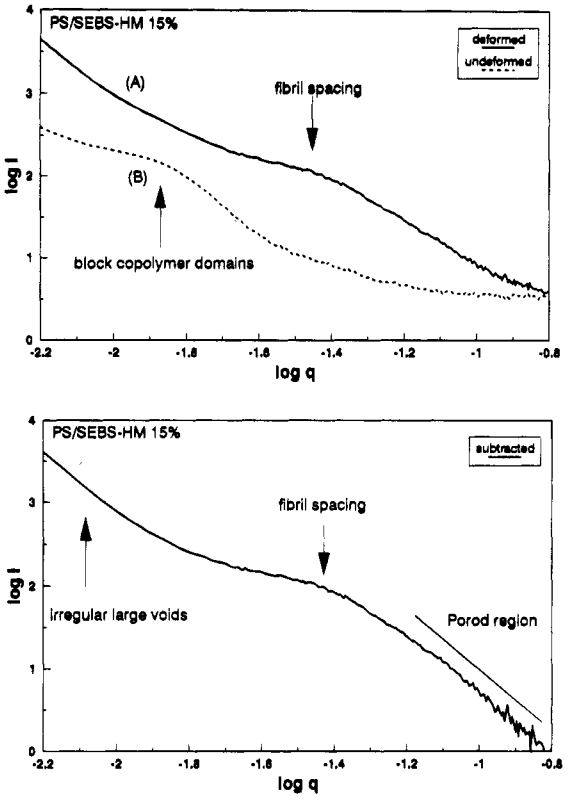


**Figure 12.** Small-angle X-ray scattering curves: (a, top) (A) PS/SEBS-HM deformed specimen with 15 wt % block copolymer (B) corresponding undeformed specimen; (b, bottom) background subtraction scattering pattern [(A) minus (B)].

deformed system is significantly above the undeformed specimen background, ensuring the accuracy of the subtraction of the background of the two-phase morphology of the material. The contribution of the block copolymer domains to the scattering pattern is negligible, as is illustrated by the scattering pattern obtained after subtraction of this contribution (Figure 12b). Further data analysis was performed on the diffraction curves whose typical form after subtraction is presented in Figure 12b.

The interference peak maximum in the scattering pattern of the undeformed specimens was identified as the manifest first scattering peak in the scattering pattern of the pure block copolymer. SAXS intensity data on pure block copolymers exhibit one to three maxima at the positions characteristic of a cylindrical geometry. The long period or microdomain spacing in the phase-separated block copolymer was estimated according to ref 40 directly from the position of the first maximum of the desmeared data and yields values of 610 and 270 Å respectively for SEBS-HM and SEBS-LM. These values were further used to estimate the size of the glassy polystyrene dispersed domains.[40,41] The values obtained are 20 and 10 nm respectively for SEBS-HM and SEBS-LM. The values of the glassy domains given by SAXS analysis are somewhat lower than the estimations from TEM micrographs (not shown), but part of the discrepancy may originate from the staining procedure.

Figure 13 illustrates the SAXS invariant treatment resulting from observation of a specimen of HIPS deformed at 5% strain. The corresponding SAXS intensity $i(q)$ profile is shown in the inset where an apparent monotonic decrease in scattered intensity occurs as a function of the scattering vector. The invariant representation of the scattering data gives a

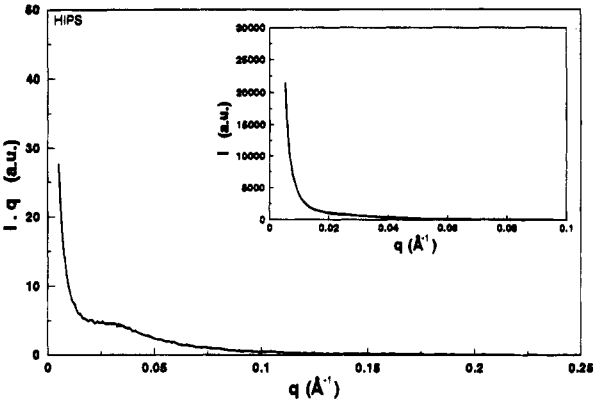


**Figure 13.** Small-angle X-ray scattering invariant for a HIPS specimen deformed at 5% extension. As an inset is shown the respective SAXS intensity profile.

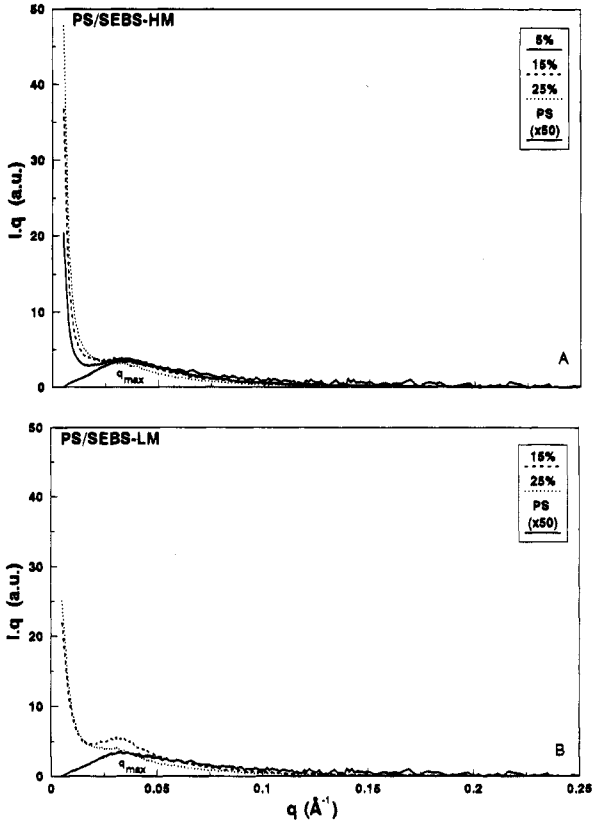


**Figure 14.** SAXS invariant of blends of SEBS-modified PS as a function of SEBS content and deformed at 5% extension ratio: (A) PS/SEBS-HM; (B) PS/SEBS-LM.

good illustration of the scattering features developed during uniaxial stretching of the specimen. The curve in Figure 13 indicates a bimodal distribution of scattering centers: an evident shoulder in the pattern occurs at the same range of $q$-values as the peak maximum in the fibril diffraction pattern reported for homopolymer polystyrene.[24] Another major component of the scattering can be discerned at smaller scattering vectors.

The scattering invariants of polystyrene homopolymer (magnified 50 times) and the respective blends with the SEBS-HM and the SEBS-LM rubbery block copolymers at different contents of rubber are shown in Figure 14. Both systems are compared over the same predetermined strain of 5%. An examination of these patterns reveals important qualitative differences between the homopolymer PS and the modified systems. The scattering curve of pure polystyrene gives evidence for the

existence of crazes[24] due to the presence of the interference peak, at $q = q_{max}$, originating from the regular spacing of polymer microfibrils and void regions across the plane of the craze. For rubber-modified PS, while the general shape of the scattering pattern remains similar with block copolymer content, major differences arise when compared with the unmodified polystyrene pattern. These latter patterns exhibit a broad interference shoulder at roughly the same scattering vector (**q**) as in pure PS. This broadening could be due to the inhomogeneous stress field around the rubber particles, causing deviation of the craze plane from the normal to the average tensile direction.[29] The dominant difference, though, comes from the strong increase in absolute intensity at very small values of **q**. The relative contribution of the scattering at low **q**-value becomes more important as the block copolymer content increases. The observed increase of the scattering intensity at very low **q**-values in the styrenic copolymer modified PS is interpreted as originating from noncrazing processes associated with irregular cavities in or around the rubbery phase. The scattering curves present the same features as the HIPS scattering profile discussed previously.

The individual contributions of these cavitational processes associated with the sharp increase in scattering intensity at very small values of **q** can hardly be estimated quantitatively due to the limited resolution in this region of the scattering. Consequently, superimposed on the fibril scattering is the high $q$-region (tail) of the scattering curve due to noncrazing scattering centers with sizes larger than the limit of the Kratky X-ray camera. This scattering tail intensity at very low **q**-values is attributed to other voiding processes, most probably cavitation within the rubber phase. The presence of a predominant noncrazing process during each stage of deformation has already been anticipated by studies using real-time small-angle X-ray scattering[9,15] on HIPS and ABS. This implies that the scattered invariant (i.e., the integration of Figures 13 and 14 over the whole $q$-range) cannot simply be used as a measure of the crazing process.

The noncrazing component of the scattering should not be included in any analysis of the crazing process. Investigations of the crazing process have concentrated on amorphous glassy polymers like polystyrene, polycarbonate, and poly(methyl methacrylate).[24,30,31] Very little has been published on the SAXS patterns of crazes in rubber-modified materials.[7-9,43] We now introduce a new method to analyze scattering patterns from rubber-modified PS, to reduce the uncertainty in the calculation of the craze fibril invariant.[44] The scattering at very low angles can be regarded as the tail portion of scattering centers (rubber cavities) whose sizes are larger than the resolution of the SAXS camera and can therefore be fitted with Porod's law. This procedure assumes only one population of crazes whose interference yields the weak maximum in the scattering pattern. After fitting the low **q**-region of the scattering curve, the contribution of this noncrazing process was subtracted from the overall diffraction pattern. Consequently, the residual scattering pattern contains the information on the craze process only. Only a small portion of the curve was fitted to obey Porod's law. A more accurate characterization of the noncrazing process would require an ultrahigh-resolution diffractometer (Bonse-Hart) which allows resolution of scattering entities of 1 $\mu$m. The fitting procedure and the total

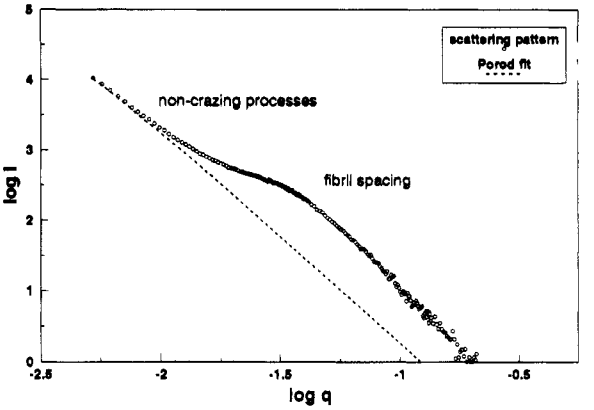


**Figure 15.** Porod region in the tail of noncrazing processes (cavitation in the rubber phase).

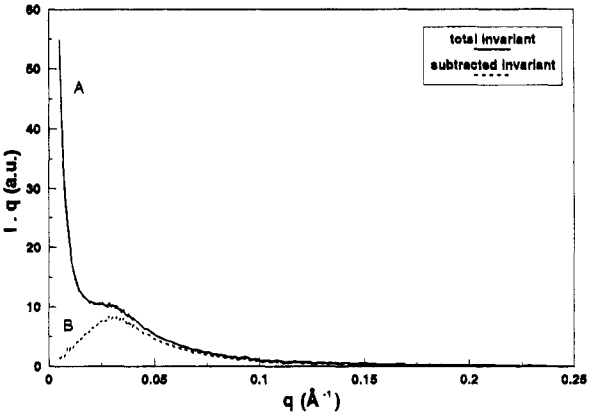


**Figure 16.** SAXS invariant: (A) recorded invariant; (B) remaining invariant after subtraction of the background due to noncrazing processes. The illustrative curves were taken for a HIPS sample deformed at 10% extension.

and corrected invariant are shown in Figures 15 and 16. This corrected scattering invariant exclusively due to fibril diffraction was used to quantify the contribution of the crazing to the deformation mechanism and to characterize the craze microstructure.

**3.4.3.2. Craze Microstructure.** Traditionally, two approaches are used to perform quantitative analyses of the craze microstructure: (1) calculation of the fibril spacing, $D_0$, directly from the scattering curve; (2) calculation of the average fibril diameter, $D$, using a Porod analysis of the high-angle portion of the scattering curve combined with the SAXS invariant. The latter method provides a more precise value of $D_0$.

Values of the mean fibril diameter were obtained using a Porod analysis of the high-angle portion of the scattering pattern exclusively due to fibril diffraction. The small-angle scattering invariant was evaluated over the corrected pattern exemplified in Figure 15, and the Porod constant, $k_1$, was obtained by extrapolating a plot of $i(q)q^3$ vs $q^3$ to $q = 0$. This curve exhibits a nearly constant value of $iq^3$ at high angles from which $k_1$ may be determined. Table 3 shows the values of the fibril diameters for the reference PS and both block copolymer modified polystyrenes.

The value of the fibril diameter, $D$, ranges from 4.5 to 5.9 nm. The important conclusion here is that essentially no difference in craze fibril diameter is observed over the range of block copolymer compositions explored for these blends. The craze fibril sizes are virtually identical for PS/SEBS-HM and PS/SEBS-LM and comparable with the homopolymer PS. The value

**Table 3. Values of the Mean Fibril Diameter of PS Modified with Different SEBS Concentrations Obtained Using a Porod Analysis**

| | $D_{\text{Porod analysis}}$ (nm) | |
|---|---|---|
| concn (%) | PS/SEBS-HM | PS/SEBS-LM |
| 0 | 5.2 | 5.2 |
| 5 | 5.0 | 5.9 |
| 15 | 4.7 | 4.9 |
| 25 | 4.5 | 5.4 |

of the average fibril diameter determined for HIPS is 6.7 nm.

If the craze fibril structure is determined using the SAXS invariant with the inclusion of the scattering contribution at low $q$ (component from voids), then the mean fibril diameter would have a strong dependence on weight fraction of the block copolymer, being in extreme about 4 times the value in pure PS for the material with 0.25 SEBS-HM. For HIPS the polymer fibril size also rises to about 15 min.

The characterization of the craze microstructure can also be roughly calculated from the interfibrillar peak maximum of the scattering curves, based on the craze model. This maximum characterizes the regular arrangement of polymer fibrils and voids in the craze network. From Bragg's law, this peak position yields a semiquantitative measure of the craze fibril spacing $D_0 \simeq 2\pi/q_{max}$. The peak position was determined based on the corrected $i(q)$ vs $q$ plot (not shown) for each system, and it follows that the fibril spacing, $D_0 \sim 24$ nm, is roughly the same for all systems and coincides with the value for the pure matrix PS. From geometric considerations it can be demonstrated[3] that for constant polymer volume during fibril drawing $D$ and $D_0$ are related through

$$D_0 = D(\lambda_{craze})^{1/2} \tag{8}$$

where $\lambda_{craze}$ is the craze fibril extension ratio.

Thus, from eq 8, the polymer fibril dimension determined for pure PS and the respective blends is $\simeq$12 nm. From the unchanged position of the peak in the typical SAXS patterns of the blends, it follows that the craze microstructure, as measured by $D$, does not vary significantly with the rubber content. This observation confirms the results found by the subtraction method. This result is important because its demonstrates that the invariant of the fibril scattering can be used to measure the total craze volume and the related plastic deformation due to crazing. This result adds confidence to the form of interpretation of the scattering curve described earlier.

An additional proof in favor of this subtraction method for obtaining the invariant exclusively due to fibril diffraction is the unchanged position of the interfibrillar peak with the block copolymer content which can be observed directly from the scattering invariant curves.

It is worth nothing that the values of $D$ determined from the Porod analysis are always smaller than the fibril diameter which could be inferred from the position $q_{max}$ of the intensity maximum and $v_f$. The Bragg's law analysis becomes increasingly inaccurate as the interfibrillar interference maximum becomes weaker and broader, as in our case. Brown and Kramer[24] advanced that, in fact, $2\pi/q_{max}$ overestimates the true $D_0$ owing to the fact that the fibril scattering intensity increases with the fourth power of the fibril size, so that the interference between the larger fibril (larger spacings) is overweighted in the scattering pattern.

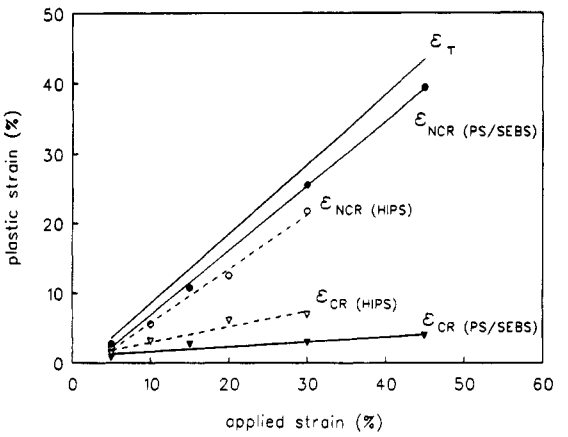


**Figure 17.** SAXS analysis of PS/SEBS-HM and HIPS at different applied strains. Plots of the total plastic strain $\epsilon_T$, noncrazing strain $\epsilon_{NCR}$ (●,○), and strain due to crazing $\epsilon_{CR}$ (▼,▽). The solid symbols correspond to PS/SEBS-HM blend and the open symbols to HIPS. The total plastic strain $\epsilon_T$ represents both systems, since the elastic contribution is essentially the same.

**Table 4. Measured Craze Strain ($\epsilon_{CR}$) and Deformation Fractions ($\epsilon_{CR}/\epsilon_T$) at Constant Extension of 5% ($\epsilon_A$) for PS/SEBS Blends ($\epsilon_T = \epsilon_A - \epsilon_{EL} = 3.5\%$)**

| | $\epsilon_{CR}$ (%) | | $\epsilon_{CR}/\epsilon_T$ | |
|---|---|---|---|---|
| concn (%) | PS/SEBS-HM | PS/SEBS-LM | PS/SEBS-HM | PS/SEBS-LM |
| 5 | 1.4 | | 0.41 | |
| 15 | 1.2 | 1.7 | 0.35 | 0.49 |
| 25 | 0.8 | 1.1 | 0.22 | 0.32 |

**3.4.3.3. Plastic Strains and Deformation Fractions.** The strain due to crazing ($\epsilon_{CR}$) at constant total plastic strain ($\epsilon_T$) was calculated from eq 4, and the results for SEBS-HM and SEBS-LM blends at different compositions with polystyrene are summarized in Table 4. The striking result in both cases is that with increasing rubber content the contribution of crazing is significantly decreasing. This effect is most pronounced in the case of the blends with SEBS-HM.

Besides the dependence of the crazing process on the rubber content, the dependence on applied strain for a particular block copolymer content of 25% by weight for the PS/SEBS-HM system was examined (Figure 17). A HIPS specimen was also studied under the same conditions at various levels of strain (Figure 17).

Both for HIPS and the PS/SEBS blend the strain due to crazing and noncrazing mechanisms increases with the extension ratio. The relative contribution of the crazing and noncrazing deformation mechanisms remains essentially the same. Although it is difficult to investigate the noncrazing process quantitatively, it can be deduced from the invariant curves (not shown) that the rubber cavitation component increases with extension ratio. The craze microstructure remains unaltered with the extension ratio.

## 4. Discussion

As expected, with increasing content of SEBS rubber in PS both the notched Izod impact strength and the strain at break increase. Based on dilatometry and TEM studies only, one could believe, following many previous studies,[3,5,10] that this increase in toughness is due to an increasing massive crazing process. However, from the SAXS studies we learned that the contribution of crazing in the glassy PS matrix *decreases* significantly with increasing rubber content at the low strain rate

investigated. Deformation studies on HIPS with RT-SAXS show that the contribution of crazing to the total plastic deformation even seems to decrease with increasing strain rate, up to impact strain rate.[15] Therefore we expect that our conclusion can be extrapolated to impact strain rates.

This result implies that the concept of multiple crazing, generated by a large amount of rubber particles, as the main source of toughness is doubtful.

The craze microstructure is independent of the type of SEBS rubber, the rubber content, and the extension ratio applied to the specimen. The measured craze fibril diameter remains constant and comparable with pure PS homopolymer. These results imply that the fibril size is a function of the matrix only, which is identical in the two materials.

Previous studies[15,24,45] report the same average value for the craze fibril diameter for polystyrene homopolymer as we found (6 nm) but systematically higher values for HIPS (typically 12−14 nm). These higher values of the fibril dimensions for rubber-modified PS have been attributed to the presence of mineral oil[46] or low molecular weight rubber components diffusing from the composite rubber particles,[47] which, at sufficiently low strain rates, would plasticize the craze fibrils.

When the complete SAXS invariant was used to characterize the craze microstructure, a significant increase in the fibril diameter was found with increasing rubber content. Because in our blends neither mineral oil nor low molecular weight rubber fractions are present, we previously advanced another explanation for this coarsening in craze microstructure with the rubber content.[48] We suggested that as a result of rubber cavitation, the craze microstructure coarsening took place because of a change in stress state in the ligaments in between cavitated rubber particles. Now we know that we overestimated the polymer fibril dimensions since the measured invariant $Q$ does include a component from voids in and around the rubbery phase. So, conversely to the previously reported coarsening of craze microstructure for rubber-modified polystyrene, with our subtraction method we found that the craze fibril structure remains comparable for both rubber-modified and unmodified PS. That means that the increase in toughness with increasing rubber content cannot be attributed to any change in the microstructure of the crazes that are produced. The craze microstructure only reflects the behavior of the PS matrix whereas the contribution of the different types of plastic deformation is associated with the rubber content and the type of rubber.

Since the increase in toughness with rubber content could not be related to an increase of the amount of crazes or to a change in craze microstructure, it should be related to an increase of another plastic deformation process. This mode of plastic deformation might be ligament shearing induced by rubber particle cavitation, although there is no firm experimental evidence for such deformation. Gilbert and Donald observed such deformation in regions ahead of a crack tip in HIPS using SEM.[14] Also in commercial HIPS the main absorption of plastic energy is the ductile deformation of the ligaments between cavitated rubber particles and not multiple crazing.

When the two types of blends with the styrenic block copolymers are compared, it is clear that PS/SEBS-HM is substantially more ductile than PS/SEBS-LM. Differences in toughness of PS/SEBS blends have usually been attributed mainly to differences in the blend morphology, which is determined by the rheological characteristics of the block copolymer relative to that of the matrix[49] or differences in mechanical adhesion toward the PS matrix[49,50] based on molecular weight differences of the PS block of the copolymer. Although we cannot neglect the differences in the shape of the dispersed phase, the dimensions of the rubbery particles are quite similar and in both cases have the required dimensions[51,52] to initiate and control crazes in PS.

When the SAXS results on the deformed PS/SEBS-HM blends are compared with those on the deformed PS/SEBS-LM blends, it turns out that the PS/SEBS-HM blends have a smaller crazing component and a significantly larger voiding component (low-angle scattering intensity) (see Table 4 and Figure 13). Thus, PS/SEBS-HM blends have a higher toughness than PS/SEBS-LM blends because they deform more through cavitation-induced ligament shearing and less through crazing.

SEBS-HM is more efficient as a toughening agent than SEBS-LM because it cavitates more easily.[53] This could originate from the difference in the internal morphology of the dispersed phase. Due to its high molecular weight, SEBS-HM has a more expanded internal morphology, a considerable lower modulus, and consequently a more elastomeric nature, which may be the cause for a lower cavitation resistance.[54]

Since the mechanical adhesion of both SEBS-HM and SEBS-LM toward PS is considerable, as shown with the peel test, we do not believe that failure at the interface plays any role in both types of blends. However, we cannot exclude that the stress transfer at the interface in the PS/SEBS-HM blends is more pronounced, which also might affect the cavitation behavior of the rubber particles.

At low strain rate the elongation at break is considerably lower for the PS/SEBS-LM blends. This can be related to the higher craze density, which increases the fracture probability.[55] In this case crazing acts as a damaging mechanism.

At high strain rates the yield stress of the PS/SEBS-LM blends is higher compared to that of the PS/SEBS-HM blends, which can be related to a higher cavitation resistance of the dispersed phase. A higher cavitation resistance and a higher yield stress of the PS/SEBS-LM blends are also responsible for a lower notched impact strength.

Blends of PS with 5% SEBS are brittle. We think this is not because the rubber particles are too small to initiate crazes[3,51,52] but probably because the rubber particle size is too small (see Table 3) to allow cavitation to occur.[56] HIPS is less ductile than a comparable PS/SEBS-HM blend, which correlates with a stronger contribution of crazing during all stages of plastic deformation (different strains). We relate this to the presence of low molecular weight components in either the PS matrix or the dispersed phase. The slight increase of fibril diameter gives some support to this idea, which will be discussed in more detail in forthcoming papers.

## 5. Conclusions

The deformation process in rubber-modified polystyrene was studied by static SAXS on deformed tensile samples under loaded conditions. The typical scattering pattern of these systems was interpreted as originating from two components: crazing in the polystyrene matrix

and a dominant cavitational component associated with the rubbery phase. We have used a new method to separate and quantify the crazing component by subtracting the contribution of the noncrazing process from the scattering invariant. We checked this procedure by comparing the values of the craze fibril diameter obtained by both the new approach and the craze peak position using Bragg's law.

The craze microstructure, as determined by the craze fibril diameter $D$, in rubber-modified PS is found to be the same as in homopolymer polystyrene (5–6 nm). With an increasing content of rubber, the amount of crazing decreases significantly whereas the (impact) toughness increases. The relative contribution of the crazing process seems to decline with the level of plastic strain imposed to the PS/rubber blends.

We believe that in both PS/SEBS blends and HIPS the main source of plastic energy absorption is microscopic shearing in the glassy ligaments in between the cavitated rubber particles (cavitation itself being an unimportant mechanism of energy dissipation). Although the evidence of extensive macroscopic shear yielding was not recognizable by dilatometry measurements, the possibility of deformation of the ligaments in between the rubber particles promoted by rubber particle cavitation may be advanced to explain the levels of toughness in these systems.[14,15] The contribution of crazing to the plastic deformation is of minor importance.

Crazing can be interpreted mainly as a damaging mechanism that should be controlled in order to prevent premature fracture.

When the blends of the two block copolymers are compared, it turns out that the crazing component is smaller and the noncrazing component is higher for blends with SEBS-HM. This result was interpreted as showing that the PS/SEBS-HM blend is tougher because it experienced more noncrazing processes, namely, cavitation-induced shear yielding, and less crazing during deformation.

**Acknowledgment.** The financial support of this work by the JNICT (Portugal) is gratefully acknowledged. This research also benefited from the use of the facilities of DSM Research (The Netherlands). Thanks to M. Walet for performing the TEM work and R. Scherrenberg for the assistance in interpreting the SAXS data. The authors wish to thank K. Dijkstra, M. Bulters, and A. Braam for many helpful discussions.

## References and Notes

(1) Kambour, R. P. *J. Polym. Sci., Part D* **1973**, *7*, 1.
(2) Kramer, E. J. *Adv. Polym. Sci.* **1983**, *52/53*, 1.
(3) Bucknall, C. B. *Toughened Plastics*; Applied Science Publishers: London, 1977; Chapter 7.
(4) Kinloch, A. J.; Young, R. J. *Fracture Behaviour of Polymers*; Applied Science Publishers: London, 1983.
(5) Bucknall, C. B. *Adv. Polym. Sci.* **1978**, *27*, 121.
(6) Kramer, E. J. Mechanisms of Toughening in Polymer Mixtures. In *Polymer Compatibility and Incompatibility—Principles and Practices*; Solc, K., Ed.; MMI Press: Midland, MI, 1982; p 251.
(7) Bubeck, R. A.; Blazy, J. A.; Kramer, E. J.; Buckley, D. J.; Brown, H. R. *Polym. Commun.* **1986**, *27*, 357.
(8) Bubeck, R. A.; Buckley, D. J.; Kramer, E. J.; Brown, H. R. *Polym. Prepr. (Am. Chem. Soc., Div. Polym. Sci.)* **1990**, *31*, 116.
(9) Bubeck, R. A.; Buckley, D. J.; Kramer, E. J.; Brown, H. R. *J. Mater. Sci.* **1991**, *26*, 6249.
(10) Beahan, P.; Thomas, A.; Bevis, M. *J. Mater. Sci.* **1976**, *11*, 1207.
(11) Keskkula, H.; Schwarz, M.; Paul, D. R. *Polymer* **1986**, *27*, 211.
(12) Cieslinski, R. 8th International Conference on Deformation, Yield and Fracture of Polymers, Preprint 85, Plastics and Rubber Institute, London, 1991.
(13) Okamoto, Y.; Miyagi, H.; Mitsui, S. *Macromolecules* **1993**, *26*, 6547.
(14) Gilbert, D. G.; Donald, A. M. *J. Mater. Sci.* **1986**, *21*, 1819.
(15) Buckley, D. J. Doctoral Thesis, Cornell University, 1993.
(16) Bucknall, C. B.; Correa, C. A.; Soares, V. L. P. ANTEC, Preprint 241, 1994.
(17) Bucknall, C. B.; Correa, C. A.; Soares, V. L. P.; Zhang, X. C. 9th International Conference on Deformation, Yield and Fracture of Polymers, Preprint 9, Plastics and Rubber Institute, London, 1994.
(18) Argon, A. S.; Salama, M. M. *Philos. Mag.* **1977**, *36*, 1217.
(19) Molau, G. E. *Block Copolymers*; Aggarwal, S. L., Ed.; Plenum Press: New York, 1970; p 79.
(20) Echte, A. *Adv. Chem.* **1989**, *222*, 15.
(21) Trent, J. S.; Scheinbeim, J. I.; Couchman, P. R. *Macromolecules* **1983**, *16*, 589.
(22) Williams, J. G. *J. Adhes.* **1993**, *41*, 225.
(23) Park, I.; Barlow, J. W.; Paul, D. R. *Polymer* **1990**, *31*, 2311.
(24) Brown, H. R.; Kramer, E. J. *J. Macromol. Sci., Phys.* **1981**, *B19*, 487.
(25) Guinier, A.; Fournet, G. *Small Angle Scattering of X-rays*; Wiley: New York, 1955.
(26) Alexander, L. E. *X-ray Diffraction Methods in Polymer Science*; Wiley: New York, 1969.
(27) Vonk, C. G. *J. Appl. Crystallogr.* **1975**, *8*, 340.
(28) Brown, H. R. *J. Polym. Sci., Polym. Phys. Ed.* **1983**, *21*, 483.
(29) Brown, H. R. *Mater. Sci. Rep.* **1987**, *2*, 31.
(30) Dettenmaier, M.; Leberger, D. *Adv. Polym. Sci.* **1983**, *52/53*, 57.
(31) Paredes, E.; Fischer, E. W. *Makromol. Chem.* **1979**, *180*, 2702.
(32) Paredes, E.; Fischer, E. W. *J. Polym. Sci., Polym. Phys. Ed.* **1982**, *20*, 929.
(33) Lauterwasser, B. D.; Kramer, E. J. *Philos. Mag.* **1979**, *39A*, 469.
(34) Beecher, J. F.; Marker, L.; Bradford, R. D.; Aggarwal, S. L. *J. Polym. Sci.* **1969**, *26*, 117.
(35) Gergen, W. P.; Lutz, R. G.; Davison, S. *Thermoplastic Elastomers. A. Comprehensive Review*; Legge, N. R., Holden, G., Schroeder, H. E., Eds.; Hanser Publishers: New York, 1987; Chapter 14.
(36) Bucknall, C. B.; Clayton, D. *J. Mater. Sci.* **1972**, *7*, 202.
(37) Bucknall, C. B.; Partridge, I. K.; Ward, M. V. *J. Mater. Sci.* **1984**, *19*, 2064.
(38) Ramsteiner, F. *Polymer* **1979**, *20*, 839.
(39) Parker, D. S.; Sue, H. J.; Huang, J.; Yee, A. F. *Polymer* **1990**, *31*, 2267.
(40) Berney, C. V.; Cohen, R. E.; Bates, F. S. *Polymer* **1982**, *23*, 1222.
(41) Richards, R. W.; Mullin, J. T. *Mater. Res. Soc. Symp. Proc.* **1987**, *79*, 299.
(42) Quan, X.; Gancarz, I.; Koberstein, J. T.; Wignall, G. D. *Macromolecules* **1987**, *20*, 1434.
(43) Steger, T. R.; Nielsen, L. E. *J. Polym. Sci., Polym. Phys. Ed.* **1978**, *16*, 613.
(44) Buckley, D. J., private communication.
(45) Brown, H. R.; Sindoni, Y.; Kramer, E. J.; Mills, P. J. *Polym. Eng. Sci.* **1984**, *24*, 825.
(46) Mills, P. J.; Brown, H. R.; Kramer, E. J. *J. Mater. Sci.* **1985**, *20*, 4413.
(47) Gebizlioglu, O. S.; Beckham, H. W.; Argon, A. S.; Cohen, R. E.; Brown, H. R. *Macromolecules* **1990**, *23*, 3968.
(48) Magalhães-Silva, A.; Borggreve, R. 9th International Conference on Deformation, Yield and Fracture of Polymers, Preprint 8, Plastics and Rubber Institute, London, 1994.
(49) Park, I.; Keskkula, H.; Paul, D. R. *J. Appl. Polym. Sci.* **1992**, *45*, 1313.
(50) Yee, A. F.; Diamant, J. *Polym. Prepr. (Am. Chem. Soc., Div. Polym. Chem.)* **1978**, *9*, 92.
(51) Donald, A. M.; Kramer, E. J. *J. Mater. Sci.* **1982**, *17*, 1765.
(52) Donald, A. M.; Kramer, E. J. *J. Appl. Polym. Sci.* **1982**, *27*, 3729.
(53) Magalhães, A.; Borggreve, R., to be published.
(54) Gent, A. N.; Lindley, P. B. *Proc. R. Soc. London* **1958**, *A249*, 195.
(55) Sjoerdsma, S. D.; Boyens, J. P. H. *Polym. Eng. Sci.* **1994**, *34*, 86.
(56) Lazzery, A.; Bucknall, C. B. *J. Mater. Sci.* **1993**, *28*, 6799.

MA950108C